Astron. Astrophys. 326, 620–628 (1997)

ASTRONOMY AND ASTROPHYSICS

Multiwavelength studies of β Cephei stars: δ Ceti

H. Cugier and D. Nowak

Astronomical Institute of the Wroclaw University, ul. Kopernika 11, PL-51622 Wroclaw, Poland

Received 22 April 1996 / Accepted 21 March 1997

Abstract. We discuss diagnostic aspects that follow from identification of the driving mechanism for the pulsation of β Cephei stars by an analysis of the well-observed star δ Ceti. Ground-based photometric and ultraviolet IUE spectro-photometric observations were used. We find that the stellar model which fits the observed frequency of oscillation and nonadiabatic observables (amplitude ratios and phase differences of the multicolour photometric measurements) describes also very well the energy flux distribution and spectral line profiles. Stellar models calculated for OPAL opacities with $Z = 0.02$ fit the observations best.

We find that δ Ceti is a star pulsating in the first overtone (p_2) of the radial ($l = 0$) mode. The luminosity of this star is in the range of $4.04 \leq \log L/L_\odot \leq 4.16$ and mass $M = 10.3 \pm 0.4$ $M_\odot$. We also discuss how these parameters can be improved using nonadiabatic observables.

Key words: β Cephei stars – stars: oscillations – stars: early-type – stars: atmosphere – stars: variable: other

1. Introduction

Recent stability surveys for stellar models corresponding to β Cephei stars performed by Dziembowski & Pamyatnykh (1993) and Gautschy & Saio (1993) leave no doubt that the κ–mechanism is responsible for the origin of pulsation of these objects. An important property of β Cephei-type oscillations is that their amplitudes are small and the linear approximation can be used. The basic aspects of such a theory are well elaborated for early-type stars, cf. Dziembowski (1994, 1995).

Cugier, Dziembowski & Pamyatnykh (1994) compared predictions of the linear nonadiabatic theory for amplitude ratios and phase differences – *the nonadiabatic observables* – with multicolour photometry and radial velocity data of β Cephei stars. The agreement is satisfactory and, in most cases, the harmonic degree l of oscillations can be determined. In particular, δ Cet is a star pulsating in the radial mode, $l = 0$. Furthermore, two-colour photometry of β Cep stars can be used to discriminate between different opacity data for modelling the internal structure of these stars, cf. Cugier et al. (1994) where the effect of using OP opacities (Seaton et al. 1994) instead of OPAL opacities (Rogers & Iglesias 1992) is illustrated. This requires spectroscopic calibration of models obtained from time-series of two-colour photometric data.

In this paper, we address these questions by detailed analysis of δ Cet (HD 16582, HR 779, B2 IV). Both the nonadiabatic observables and mean stellar parameters are investigated using ground-based photometric data and UV spectro-photomeric observations collected by the International Ultraviolet Explorer (IUE) satellite.

Send offprint requests to: H. Cugier

2. Oscillation parameters

2.1. Period

δ Ceti belongs to a group of well-observed β Cephei stars. Extensive multicolour Strömgren photometry is presented by Jerzykiewicz et al. (1988). This star has sinusoidal light curves with period $P = 0.^{\rm d}161137$. Unlike most other β Cephei stars, δ Cet does not show multiple periods or multiple line–profile variations. A hypothetical secondary short-period component, which may be responsible for a marginal night-to-night variation of this star, indicates an amplitude not exceeding $0.^{\rm m}0016$, cf. Jerzykiewicz et al. (1988). In the case when only one mode of oscillation is known, pure frequency measurements are not sufficient for unique selection of the stellar model despite identification of the harmonic degree l. This is illustrated in Fig. 1, where the diagram $\log g \; vs \; \log T_{\rm eff}$ is plotted for stellar models with $M = 8 - 16$ $M_\odot$ (thin lines) calculated for OPAL opacities with metal content parameter $Z = 0.02$. The initial hydrogen and helium abundances were adopted as equal to $X = 0.70$ and $Y = 0.28$, respectively. In Fig. 1, stellar models showing unstable p_1 and p_2 radial modes with period exactly the same as observed for δ Cet ($P = 0.^{\rm d}161137$) are indicated as thick lines with filled circles for OPAL opacities and thin lines with open circles for OP opacities, respectively. As one can see, models corresponding to p_1 and p_2 are shifted in $\log g$ by about 0.13 dex. Use of OP opacities instead of OPAL opacities results in higher effective temperature for the investigated star, cf. Fig.

1. One can therefore conclude that the proper selection of the stellar model is possible if such parameters as P, $T_{\rm eff}$ and $\log g$ are known with good precision for this star.

2.2. Nonadiabatic observables

The nonadiabatic observables, mentioned in Sect. 1, are the amplitude ratios and the phase differences for various oscillating parameters. We rely on results of model calculations made by Cugier at al. (1994) for photometric data and readers are referred to that work for details. This task involves recent results of stellar evolution calculations and linear nonadiabatic pulsation theory (both taken from Dziembowski and Pamyatnykh's 1993 survey), and well-known stellar atmospheres models (line-blanketed Kurucz's 1979a, b data). Fig. 2a and b show the nonadiabatic observables, viz. Colour amplitude / Visual amplitude $vs.$ Colour phase - Visual phase for models calculated with OPAL and OP opacities. The lines correspond to unstable p_1 and p_2 radial modes with period equal to $0.^{\rm d}161137$.

According to Jerzykiewicz et al. (1988), the phase lag between the light and radial velocity curves is equal to $0.200 \pm 0.005P$, and no compelling evidence for variation of this quantity was found. The epochs of maximum light are not entirely independent of wavelength. The u curve lags behind the v, b and y curves by about $0.013P$, cf. Jerzykiewicz et al. (1988). Fig. 2c and d show that observed phases of the flux maximum (starred symbols) as a function of wavelength offer determination of the effective temperature of δ Cet with high precision. The step in $\log T_{\rm eff}$ of the stellar models shown in these figures is equal to 0.005 dex. Using OPAL opacities with Z = 0.02, the observed amplitude ratios and the phase differences lead to the nonadiabatic model shown in Cugier's et al. (1994) Table 2. In particular, the best fit model predicts $\log T_{\rm eff}$ = 4.347 and $\log g$ = 3.73. These values should be verified by "classical" methods of determination of $T_{\rm eff}$ and $\log g$.

3. Mean stellar parameters

No empirical effective temperature in the sense of the method elaborated by Code et al. (1976) is available for δ Cet. There are several indirect ways of estimating the effective temperatures of stars. These methods use some properties of the spectrum such as the slope of continuum over a limited wavelength interval or the relative strengths of absorption lines from elements present in two or more stages of ionization to identify a star with a model atmosphere. The effective temperature of the model atmosphere which gives the best representation of the observed data is said to be equivalent to the effective temperature of a star.

One of the efficient methods of estimating the atmospheric parameters is based on the Strömgren–Crawford $uvby\beta$ photometric system. Two indices, c_1 and $[u-b]$, are used to derive the effective temperature of early-type stars. Although the $[u-b]$ index is a more sensitive indicator of $T_{\rm eff}$, there are reasons for preferring the c_1-index as a temperature indicator, cf. Shobbrook (1976) and Davis & Shobbrook (1977). These reasons appear to originate in a metal-line index m_1 involved in the definition of

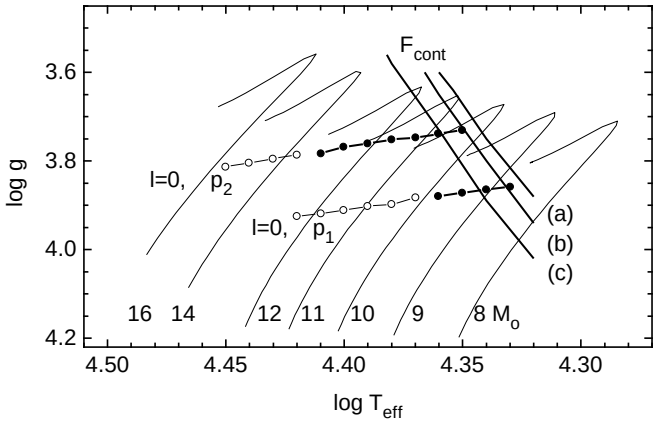

Fig. 1. The diagram $\log g$ vs. $\log T_{\rm eff}$ for stellar models of M = 8 − 16 $M_\odot$ during the Main Sequence phase of evolution (thin lines). Models showing unstable radial modes with period $0.^{\rm d}161137$ are plotted as thick lines with filled circles (for OPAL opacities) and thin lines with open circles (for OP opacities), respectively. Lines marked as $F_{\rm cont}$ indicate the models best fitting the observed energy flux distribution. The lines a, b and c correspond to $E(B-V) = 0.^{\rm m}014$, $0.^{\rm m}020$ and $0.^{\rm m}030$, respectively.

$[u-b] = 2\,[m_1] + [c_1]$. A further argument for c_1 as an effective temperature indicator follows from an inspection of the theoretical $uvby\beta$ indices calculated for the older (Kurucz 1979a, b; Lester et al. 1986) and the latest (Kurucz 1991) line-blanketed models of atmospheres. Since the new models were obtained for upgraded stellar opacities, such a comparison gives insight to sensitivity of the photometric indices to uncertainties in the line blanketing effects. As one can expect, the c_1 index is much less sensitive to changes in stellar opacities than the $[u-b]$ one. We found the difference of $\Delta c_1 = \pm 0.^{\rm m}003$ between the old and new models, which corresponds to $\Delta\ T_{\rm eff} = \pm 110$ K for a star with $T_{\rm eff}$ = 25000 K and $\log g$ = 4.0. This effect is small in the context of the present paper, but using the new c_1-indices has an important advantage: they are calculated for a grid of models with step 1000 K in $T_{\rm eff}$ near 25000 K, whereas the step in the older grid is equal to 2500 K. We therefore derived the effective temperature and surface gravity from the original $uvby\beta$ data of δ Cet using c_1- and β-indices given by Kurucz (1991) and Smalley & Dworetsky (1995), respectively. Unfortunately, this is not entirely a consistent approach, because the β index corresponds to the older grid of models (the new Kurucz (1991) data do not contain the β index). However, due to the fact that the theoretical β indices are calibrated to observations of standard stars (cf. Smalley & Dworetsky 1995), one can expect that the final result is only little influenced by this quasi-homogeneous approach. The results are shown in Table 1. Following Shobbrook (1978), we adopted the relations $(b-y)_o = 0.099c_o - 0.117$ and $E(c_1) = 0.24\,E(b-y)$ in the de-reddening procedure. Stellar parameters derived from the calibration formulae given by Napiwotzki et al. (1993) and Balona (1994), which are based on the $[u-b]$ and c_1 indices, respectively, are also shown in Table 1. As one can see, for a given set of observations, Napiwotzki's et al. (1993)

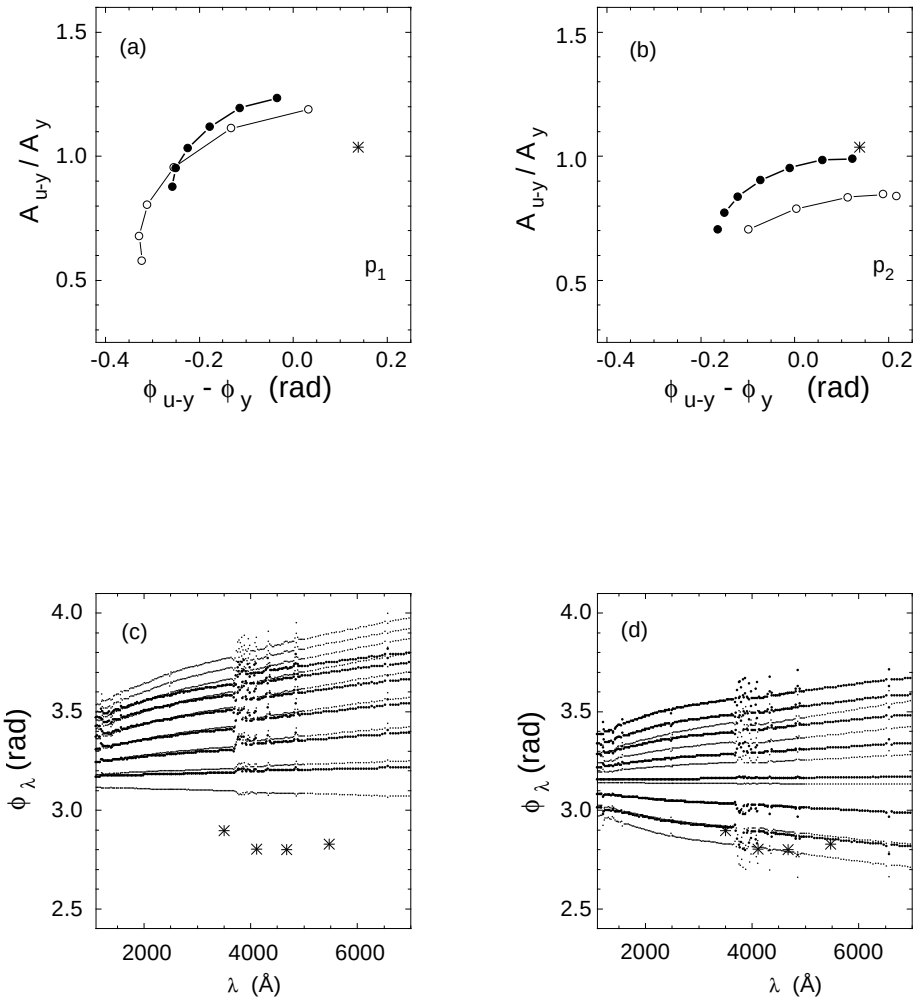

Fig. 2. a Nonadiabatic observables of δ Cet (starred symbols) on the diagram colour to light amplitude ratio vs. phase difference. The lines correspond to an unstable p_1 radial mode with period exactly the same as observed for this star (P = 0.$^{\rm d}$161137). Stellar models calculated by Dziembowski and Pamyatnykh (1993) for OPAL (thick lines with filled circles) and OP (thin lines with open circles) opacities with Z = 0.02 are shown. **b** The same as Panel a but for stellar models calculated for unstable p_2 radial mode. **c** The observed (starred symbols) phases of light maxima are plotted together with nonadiabatic models displayed in Panel **a**. **d** The same as Panel **c** but for stellar models shown in Panel **b**.

Table 1. log $T_{\rm eff}$, log g and E($b-y$) derived from $uvby\beta$ photometry.

c_1	$(b-y)$	β	Ref.	c_o	log $T_{\rm eff}$			log g	E($b-y$)
					[4]	[5]	[6]	[6]	[6]
0.082	-0.102	2.624	[1]	0.080	4.335	4.345	4.340	3.84	0.007
0.105	-0.099	2.613	[2]	0.103	4.329	4.307	4.321	3.54	0.008
		2.621	[3]	0.091^a		4.332	4.331	3.73	0.008^a

References for c_1, $(b-y)$ and β:
[1] Lindemann & Hauck (1973), [2] Shaw (1975), [3] and ^{a}) Shobbrook (1978)
References for $T_{\rm eff}$:
[4] Napiwotzki et al. (1993), [5] Balona (1994), [6] this paper

formula and our approach give the same results for $T_{\rm eff}$ within an error box of $\pm$0.01 dex. Similar scatter is present when different data are adopted for the mean photospheric indices of δ Cet with the exception of numbers obtained from the two-parametric formula given by Balona (1994), cf. Table 1. A direct interpolation in the theoretical grid of indices is recommended. It is interesting to note that the effective temperature derived from the photometric indices is in good agreement (again within the error box of $\pm$0.01 dex.) with the temperature obtained from the nonadiabatic observables discussed in Sect. 2.2.

Recently, Kolb & Baade (1994) reported a log g determination for δ Cet from an analysis of the H_γ line. They found log g = 3.70 $\pm$ 0.25 for $T_{\rm eff}$ = 21000 K. The error $\pm$ 0.25 in log g is mainly due to assumed uncertainty in the effective temperature of the order of 2000 K.

Table 2. Journal of the IUE observations.

Image no.	Disp.	U.T.	Date	JD Hel. 2440000.0+	ϕ	Exp.	Max. DN or C,B
SWP 4482	H	21^h44^m	1979 Mar, 4	3937.4056	.2813	50^s	130
SWP 4483	H	22 15	1979 Mar, 4	3937.4271	.4149	75	255
SWP 4484	H	22 48	1979 Mar, 4	3937.4500	.5571	65	250
SWP 4485	H	23 19	1979 Mar, 4	3937.4715	.6907	50	205
SWP 4486	H	23 49	1979 Mar, 4	3937.4924	.8200	50	210
SWP 4487	H	00 19	1979 Mar, 5	3937.5132	.9493	50	205
SWP 4488	H	00 50	1979 Mar, 5	3937.5347	.0829	50	215
SWP 4489	H	01 21	1979 Mar, 5	3937.5563	.2165	50	205
SWP 4490	H	01 51	1979 Mar, 5	3937.5771	.3458	50	190
SWP 4491	H	02 22	1979 Mar, 5	3937.5986	.4794	50	200
SWP 4492	H	02 53	1979 Mar, 5	3937.6201	.6130	50	205
SWP 4493	H	03 23	1979 Mar, 5	3937.6410	.7423	50	215
LWP 6341	H	13 24	1985 Jul, 4	6251.0583	.4791	30	225, 47
SWP 29807	L	02 10	1986 Dec, 5	6769.5903	.4100	2	209, 17
LWP 9634	L	02 44	1986 Dec, 5	6769.6139	.5565	1	187, 33
SWP 29808	L	02 54	1986 Dec, 5	6769.6208	.5996	2	220, 17
LWP 9635	L	03 55	1986 Dec, 5	6769.6632	.8625	1	197, 34
SWP 29809	L	04 06	1986 Dec, 5	6769.6708	.9099	2	233, 18
LWP 9636	L	05 11	1986 Dec, 5	6769.7160	.1901	1	197, 34
SWP 29810	L	05 22	1986 Dec, 5	6769.7236	.2375	2	247, 18
LWP 9637	L	06 22	1986 Dec, 5	6769.7653	.4960	1	195, 37
SWP 29811	L	06 32	1986 Dec, 5	6769.7722	.5391	2	236, 18
SWP 29812	L	07 22	1986 Dec, 5	6769.8069	.7546	2	228, 19
SWP 29813	L	07 57	1986 Dec, 5	6769.8313	.9055	2	247, 18
SWP 29814	L	08 32	1986 Dec, 5	6769.8556	.0563	2	250, 19

4. IUE observations

The IUE observational material of δ Cet consists of low and high resolution spectra, archived by the ESA Observatory at VILSPA. The images, listed in Table 2, were taken by means of the short-wavelength primary (SWP) and long-wavelength primary (LWP) cameras with high (H) and low (L) resolution modes. The pulsation phases were calculated from the following parabolic ephemeris:

T(max. light) = HJD 2438385.6888 + 0.16113713 E + 11.7 10^{-12} E^2

describing moments of the maximum light of this star (cf. Jerzykiewicz et al. 1988). The last column of Table 2 shows an exposure classification code. The VILSPA code is given by a single number corresponding to the maximum Digital Number (DN) of expositions (the saturated level occurs at DN = 255), whereas the GSFC data show both the continuum (C) and background (B) levels in DN units, respectively.

The analysed images are well exposed, and we used IUE programs developed for PC computers consisting of several graphical subroutines useful for analysis of the extracted data from the standard IUE SIPS reduction procedure. One of the advantages of our software is the possibility to select the best fit parameters for removing the blaze function of the echelle grating to improve the standard ripple correction of the high resolution images.

5. Analysis of the continuum flux distribution

All of the low-resolution spectra of δ Cet were obtained in a trailed mode and therefore cannot be calibrated in absolute units. For the same reason, the observational material cannot be used to investigate the UV light curves during the pulsation cycle. We therefore analysed the phase-averaged observations. For this purpose, we constructed the mean energy flux distribution by co-adding all of the low-resolution images for a given camera. We first filtered short and long wavelength images by a five-point filter with least–squares weights and fitted them, in the sense of the minimum least-square deviations, to SWP 29811 and LWP 9636 images, respectively. As one can see from Table 2, there are 8 low-resolution SWP images symmetrically distributed over pulsating phases. In particular, 3 images (SWP 29807, 29808 and 29811) were taken at $\phi = 0.4 - 0.6$, whereas another 3 images (SWP 29809, 29813 and 29814) at $\phi = 0.9 - 0.0 - 0.1$. The remaining two observations were obtained at $\phi = 0.2375$ (SWP 29810) and $\phi = 0.7546$ (SWP 29812), respectively. We therefore calculated the mean spectrum, assuming the same weights for all the low-resolution SWP images. In the case of the low-resolution LWP images taken at $\phi = 0.1901, 0.4960, 0.5565$ and 0.8625, we first derived the mean spectrum from observations at $\phi = 0.4960$ and 0.5565, and then calculated the arithmetic mean spectrum for this camera. These observational data are supplemented by the ground-based observations from 3300 Å to 6050

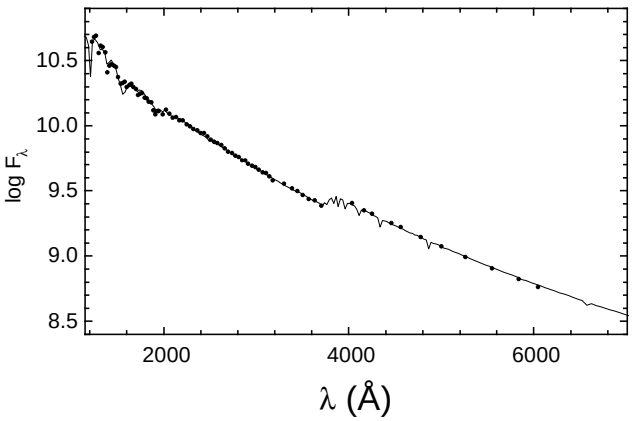

Fig. 3. The best fit of the predicted flux of radiation (continuous line) to IUE and visual observations of δ Cet (points).

Å made by Schild et al. (1971). Thus the analysed energy flux distribution of δ Cet contains UV and visual observations in the form of three pieces of the spectrum corresponding to wavelength regions 1200 - 1950 Å, 1900 - 3200 Å and 3300 - 6050 Å, respectively.

Next, the observed flux distribution was dereddened by means of the mean extinction curve given by Savage & Mathis (1979). As the first approach, we adopted the extinction curve corresponding to E($B-V$) = 1.7 E($b-y$) = 0.$^{\rm m}$014. The last equality corresponds to E($b-y$) = 0.$^{\rm m}$008 shown in Table 1. Having dereddened flux distribution, we searched for the best fit of the theoretical flux to the observed one, in the least-squares sense, by adjusting log $T_{\rm eff}$ and log g. During this procedure, we also introduced two additional parameters to make an agreement in the continuum levels of the three regions of the spectrum mentioned above. Theoretical fluxes were interpolated from the published Kurucz (1979a, b) grid of models with a solar abundance of elements. According to Buser & Kurucz (1992), the Kurucz (1979a, b) grid of models for O to G stars together with the new models for F- to K-stars (Kurucz 1991) provide an extensive, quasi-homogeneous grid of low-resolution theoretical flux spectra for a significant range of stellar parameters, covering most of the observed HR diagram. We found the best fit solution for log $T_{\rm eff}$ = 4.354 and log g = 3.63, but an almost equally good fit (in the sense of the least-squares deviations) exists for a sequence of models shown in Fig. 1. The results are most sensitive to the adopted value of E($B-V$), cf. Fig. 1, where solutions corresponding to E($B-V$) = 0.$^{\rm m}$020 and 0.$^{\rm m}$030 are also plotted. An increase in E($B-V$) from 0.$^{\rm m}$014 to 0.$^{\rm m}$030 results in Δ log $T_{\rm eff}$ = 0.02 and Δ log g = 0.15, which can be regarded as error boxes for these photospheric parameters derived from the observed slope of the continuum. The best fit solution with E($B-V$) = 0.$^{\rm m}$014 is displayed in Fig. 3.

Similar analysis was made for the high-resolution images of δ Cet. Also in this case, only relative energy flux distributions can be studied, but now due to the small aperture used, with the exception of the LWP 6341 image. The carefully reprocessed images were pre-filtered by a 121-point running mean filter reducing the spectral resolution to about 5 Å, comparable with the low-resolution IUE observations. These spectra (cf. Table 2) were obtained with a time step of about 30 min and are well distributed over the pulsating phase. The mean spectrum was therefore calculated with the same weights for all images. No important discrepancy was found between the two sets of data for the continuum flux distribution, although using high-resolution images and assuming E($B-V$) = 0.$^{\rm m}$014 the best fit solution exists for slightly different parameters of log $T_{\rm eff}$ = 4.378 and log g = 3.67. These values however are within the error boxes (Δ log $T_{\rm eff}$ = $\pm$0.02 and Δ log g = $\pm$0.15) estimated from the analysis of the low-resolution spectra of δ Cet.

Now, we examined how well the phase-averaged energy flux distribution represents the steady state model. For this purpose, theoretical fluxes generated for a nonadiabatic model of δ Cet (cf. Sect. 2.2) at pulsating phases ϕ = 0.1 n (n=0,...,9) were used to construct the mean flux (in logarithmic scale) and compared with the flux distribution corresponding to the steady-state model. We found the differences less than 0.0006 dex. in the considered wavelength region.

6. Analysis of line profiles

6.1. Mean spectrum of δ Cet

High-resolution images were used to study line profiles of selected species. First, we constructed the mean spectrum of δ Cet, because one can expect small pulsational effects in moderate 0.2 Å-resolution observations collected by the IUE satellite. The procedure was similar to the one described in Sect. 5, but now small corrections to wavelengths derived by a cross-correlation method were applied for individual spectra. Having already established photospheric parameters log $T_{\rm eff}$ = 4.35$\pm$0.02 and log g = 3.73$\pm$0.15, we examined how LTE theoretical spectra fit the mean high-resolution spectrum of δ Cet. For this purpose, the solar chemical composition of elements was adopted from Kurucz's (1979a) data, i.e., the carbon and silicon abundances were taken as equal to log N(C)/N$_{\rm tot}$ = -3.48 and log N(Si)/N$_{\rm tot}$ = -4.50, respectively. The results are plotted in Fig. 4 for hydrogen, carbon and silicon lines listed in Table 3. Damping constants for the Stark broadening of the line absorption coefficients used in the calculations were taken from Stehle (1994) for the H I Ly$_\alpha$ line and Sahal-Brechot & Segre (1971) for carbon and silicon lines. We assumed the microturbulent velocity ξ=0 and the rotational velocity of δ Cet equal to V_e sin i = 15 km s^{-1} (cf. Gies & Lambert 1992). An increase in ξ to 2 km s^{-1} as in Kurucz's models of atmospheres has negligible effect on the analysed lines, which are located at the damping part of the curve of growth. The dotted line in Fig. 4a shows the photospheric flux near λ 1200 Å, whereas the synthetic spectrum including the interstellar component of H I Ly$_\alpha$ is shown as the solid line. The additional interstellar component was taken into account as described by Jenkins (1970). We found the hydrogen interstellar column density equal to N(H I) = 1.0 10^{20} cm^{-2}. This is in good agreement with the E($B-V$) value discussed in Sect.

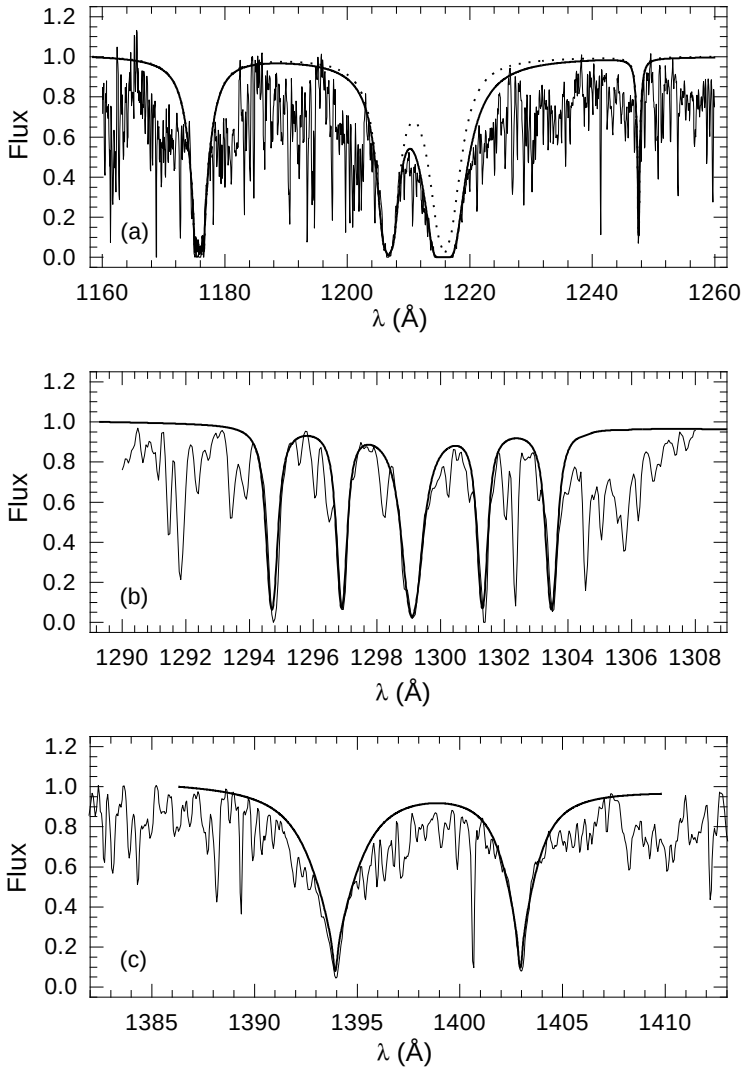

Fig. 4a–c. Mean high-resolution IUE spectra (thin lines) are compared with theoretical ones calculated for an atmospheric model of $\log T_{\rm eff} = 4.347$, $\log g = 3.73$, ξ=0, $V_e \sin i = 15$ km s^{-1} and solar abundance of elements. Panel **a** shows synthetic spectra of C III 1175 Å, Si III 1206 Å, H I Ly$_\alpha$ 1216 Å and C III 1247 Å lines (see text), Panel **b** displays Si III lines near 1300 Å and Panel **c** illustrates Si IV lines near 1400 Å, respectively. The spectra are normalized to the theoretical continuum flux level.

4.1. Using the calibration of E($B-V$) vs. log N(H I) given by Bohlin et al. (1978), one can find E($B-V$) = 0.$^{\rm m}$02.

6.2. Line profile behaviour during pulsation cycle

In this section, we report the comparison of the individual high-resolution images of δ Cet (cf. Table 2) with the model predictions for different pulsational phases. Theoretical profiles were calculated as described by Cugier (1993), taking into account geometrical, temperature and pressure effects in specific intensity variations on the stellar surface during the pulsation cycle. The Doppler broadening due to the velocity field of a pulsating and rotating star is also included. In this paper, the original computing code was modified in agreement with the nonadiabatic (temperature and pressure) effects described by Cugier et al. (1994). The amplitude of the stellar radius variations of δ Cet was obtained by normalizing the predicted amplitude A_y to the observed one. Thus we have self-consistent data for both continuum and line profile variations as functions of pulsation phase. Having already established the stellar nonadiabatic model (cf. Sect. 4) and parameters involved in the analysis of the mean line profiles (cf. Sect. 6.1), no additional parameters in model calculations for different pulsation phases are needed. We examined the behaviour of Si III 1300 Å and Si IV 1400 Å lines and found satisfactory agreement with the observations. As an example, Fig. 5 shows the Si III 1300 Å lines for the first 8 high-resolution images listed in Table 2. As one can see, the fit quality is basically the same as in Fig. 4, although the noise in the observed data is larger.

In Sect. 6.1, we analysed the mean spectrum of δ Cet averaged over the pulsating phases. The question is how well this spectrum describes the steady-state model corresponding to this star. We repeated exactly the same procedure as for the observed mean spectrum of δ Cet, but for the theoretical spectra presented here. The mean theoretical spectrum was then compared with the steady-state model. We found the differences in the line profiles less than 0.1 per cent, with the exception of the line cores where the differences reach about 3 per cent. It results in changes of total equivalent widths of the Si III lines near 1300 Å (as measured from 1292 Å to 1306 Å) by about 0.5 per

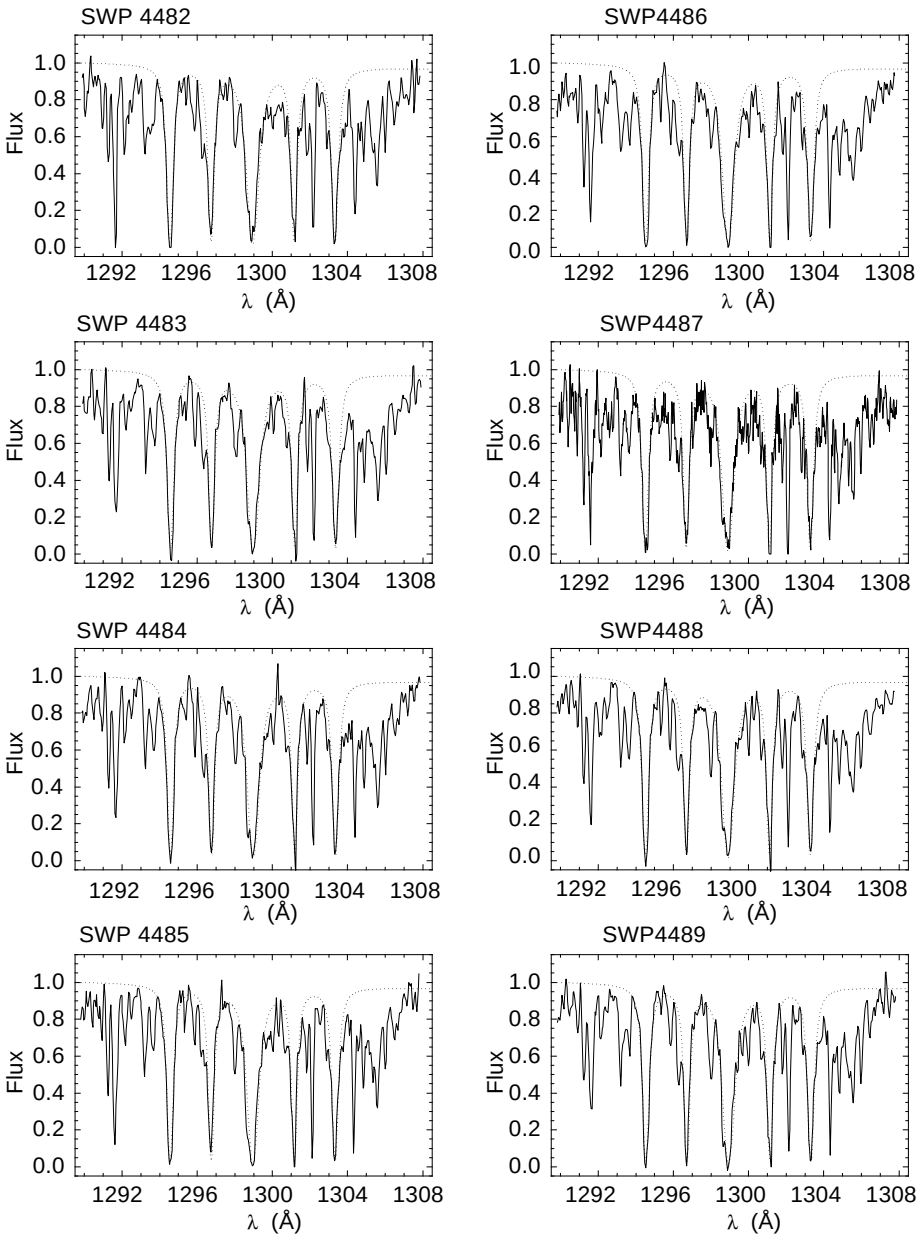

Fig. 5. Si III 1300 Å line profile behaviour during the pulsating cycle. The predicted spectra (dotted lines) correspond to a stellar model of log $T_{\rm eff}$ = 4.347, log g = 3.73, ξ = 0, log N(Si)/$N_{\rm tot}$ = -4.50 and V_e sin i = 15 km s^{-1}.

cent. This indicates that the procedure used in Sect. 6.1 is well justified to study the steady-state model corresponding to δ Cet.

7. Luminosity, mass and age

The diagram plotted in Fig. 6 shows the luminosity $vs.$ mean stellar density for models of M = 9, 10, 11 and 12 $M_\odot$ calculated by Dziembowski & Pamyatnykh (1993) using OPAL opacities with Z = 0.02. Stellar models corresponding to the parameters (4.33 $\leq$ log $T_{\rm eff}$ $\leq$ 4.37 and 3.58 $\leq$ log g $\leq$ 3.88) derived from spectro-photometric observations of δ Cet (cf. Sect. 5) are indicated by dots. Knowledge of the mode of oscillation (l = 0, p_2) leads to a mean stellar density equal to $< \rho >= \pi/(G\sigma^2 P^2)$ = 0.0379 g cm^{-3}. Because the oscillation period P is known with high precision, the accuracy of $< \rho >$ is determined by the error in the nondimensional frequency σ, which increases slightly during the envelope expansion phase of M-S stellar evolution, cf. Dziembowski & Pamyatnykh (1993). In the range of log $T_{\rm eff}$ and log g considered, $\Delta < \rho > / < \rho >= \Delta\sigma/\sigma = \pm 0.006$. This restricts the possible solutions to the narrow region around the vertical line shown in Fig. 6. The condition that only unstable models for the first overtone of the radial mode should be considered leads to 4.043 $\leq$ log $L/L_\odot$ $\leq$ 4.164 for δ Cet. Both $< \rho >$ and log L are almost insensitive to moderate changes in chemical composition of stars, due to the fact that the effect of the increase in mean molecular weight (accompanied by decrease of the stellar radius) is well compensated by the effect of the decrease in M. For instance, the increase in Z from 0.02 to 0.03 is compensated by the decrease in mass by about 6 per cent for

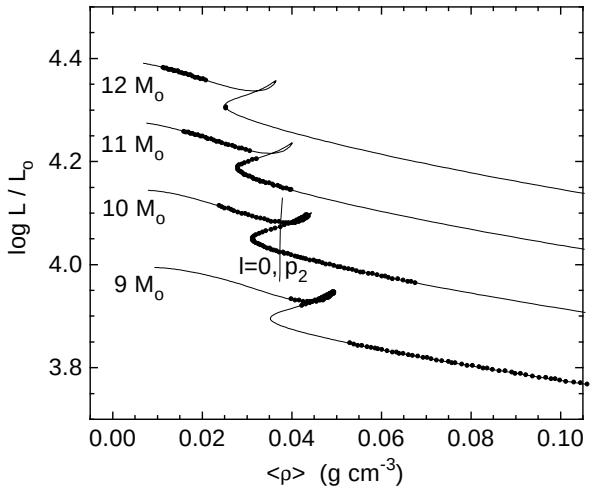

Fig. 6. The diagram log $L/L_{\odot}$ vs. $< \rho >$ for stellar models of M = 9 − 12 M$_{\odot}$ calculated by Dziembowski & Pamyatnykh (1993). Models with log $T_{\rm eff}$ = 4.35 ± 0.02 and log g = 3.73 ± 0.15 are shown as dots. The vertical line indicates possible solutions for δ Cet oscillating in (l = 0, p_2) mode.

Table 3. Atomic data of selected lines.

Ion	λ_{ij} [Å]	g_i	E_i [cm^{-1}]	f_{ij}
H I	1215.67	2.	0.	0.4162
C III	1174.92	3.	52390.	0.118
	1175.25	1.	52367.	0.275
	1175.57	3.	52390.	0.070
	1175.70	5.	52447.	0.212
	1175.97	3.	52390.	0.089
	1176.35	5.	52447.	0.069
C III	1247.37	3.	102351.	0.164
Si III	1206.50	1.	0.	1.690
Si III	1294.54	3.	52853.	0.235
	1296.73	1.	52725.	0.565
	1298.89	3.	52853.	0.141
	1298.96	5.	53115.	0.423
	1301.15	3.	52853.	0.188
	1303.32	5.	53115.	0.140
Si IV	1393.76	2.	0.	0.528
	1402.77	2.	0.	0.262

M-S stellar models with X = 0.70. Similar behaviour is seen when X changes.

Another uncertainty in stellar evolution theory is connected with treatment of the convective overshooting phenomenon. Models plotted in Fig. 6 were calculated with no convective overshooting and no mass loss during evolution. As pointed out by Dziembowski & Pamyatnykh (1993), such models are not in conflict with the positions of β Cep stars on the H-R diagram. There are however motivations for considering these effects on stellar evolution, cf. e.g., Claret & Gimenez (1992), Schaller et al. (1992) and Bressan et al. (1993), where results for a moderate convective overshooting calculated using the OPAL opacities are given. Mass loss by radiatively-driven stellar wind was included in these calculations. One can estimate from these data that, for stellar parameters corresponding to δ Cet, the convective overshooting effect results in higher luminosity by about 0.05 dex., which again can be compensated by a decrease in mass of about 2 per cent. The effect of mass loss is about one order of magnitude smaller. The mass of δ Cet is estimated as $M = 10.3 \pm 0.4$ M$_{\odot}$, and the age is probably in the range from log(Age) = 7.225 to 7.38 y, as indicated by Dziembowski & Pamyatnykh's (1993) and Schaller's et al. (1992) models, respectively.

The convective overshoot has little effect on the nondimensional frequencies of the radial modes, cf. Dziembowski & Pamyatnykh (1991, 1993). In this case, a detailed analysis of stars located very near the low-temperature boundary of the M-S region may shed some light on this question. On the other hand, Dziembowski & Pamyatnykh (1991) showed that g-modes which enter the p-mode frequency range during stellar evolution become partially trapped in the region containing the outer part of the convective core and the chemically inhomogeneous zone left behind by the shrinking core. Frequencies of such modes are sensitive to the treatment of the convective core boundary. Thus, the detection of the g_1-mode (cf. Dziembowski & Pamyatnykh 1993) in β Cep stars would give an important tool for testing stellar theory.

We add that the effect of changing the chemical composition and stellar opacity data, as well as convective overshooting effect, cannot be exactly compensated for by a change of mass. The nonadiabatic parameters $\tilde{f}$ and ψ change rapidly with $T_{\rm eff}$, but they are also sensitive to log g, Z and stellar opacity sources, cf. Cugier et al. (1994). These quantities are closely linked to the driving mechanism of stellar pulsations and together with the nonstability criterion are very useful for testing the stellar models. All these circumstances lead us to the conclusion (cf. Sect. 2) that stellar models calculated with OPAL opacities for the initial chemical composition X = 0.70, Y = 0.28 and Z = 0.02 fit best the observations of δ Cet. Having established chemical composition and opacity data, nonadiabatic observables offer determination of the effective temperature and luminosity with high precision. Fig. 2 shows that $\tilde{f}$ and ψ transformed to observed parameters lead to a shift of the maximum light by about ±0.1 rad for $\Delta T_{\rm eff}$ = ±0.005 dex, whereas the observed phase lag between light and radial velocity curves seems to be known with an accuracy of the order of ±0.005 P = ±0.03 rad, cf. Jerzykiewicz et al. (1988). In the case of log $T_{\rm eff}$ = 4.347 ± 0.005, one can therefore obtain log $L/L_{\odot}$ = 4.07 ± 0.03 for δ Cet. However, further tests performed for other β Cep stars are needed to establish the final calibration of the stellar opacity data.

8. Conclusions

Pulsation data for β Cephei stars are an important source of information about the considered objects. These data consist of

periods of oscillation and nonadiabatic observables, which are related to the eigenvalues and eigenfunctions of nonadiabatic oscillations, respectively. The nonadiabatic observables, $\tilde{f}$ and ψ, change markedly with $T_{\rm eff}$, Z and depend on the stellar opacity data used, cf. Cugier et al. (1994). In this paper, an attempt was made to calibrate these data using both time-series photometric data and spectro-photometric observations corresponding to the mean stellar state of δ Cet.

We found that the model calculated with the OPAL opacities for log $T_{\rm eff}$ = 4.347, log g = 3.73 and Z = 0.02 describes very well the observed properties of the analysed star. This model, obtained from the analysis of time-series of the multicolour $uvby$ photometric data, describes also very well the observed UV and visual energy flux distribution, as well as line profiles taken in the high-resolution mode. In other words, this model is located well within error boxes derived from "classical" spectro-photometric analysis of δ Cet. Models based on OP opacities predict too high an effective temperature and fit markedly worse these observations.

Having established chemical composition and opacity data, nonadiabatic observables offer determination of the effective temperature and luminosity with high precision, viz., log $T_{\rm eff}$ = 4.347 ± 0.005 and log $L/L_{\odot}$ = 4.07 ± 0.03 for δ Cet. Thus the data of individual β Cep stars may be used for precise determination of the distances of these objects. At the moment, this solution must be treated with caution, because the calibration procedure should first be extended for a number of β Cep stars. A more realistic estimation is therefore $4.04 \leq \log L/L_{\odot} \leq 4.16$, which is consistent with both OPAL and OP opacities. This estimation is also insensitive to moderate chemical composition changes and is not significantly influenced by uncertainties in description of the convective overshooting effect.

New aspects also arise for spectroscopic studies. Determination of the chemical composition of β Cephei stars is an important point, due to the large sensitivity of the oscillation parameters to the stellar opacities. We found that the calculated spectra fit very well the observed C III, Si III and Si IV line profiles of δ Cet, assuming solar abundance of carbon and silicon. This is in agreement with the conclusion derived from the nonadiabatic observables (cf. Sect. 2). This is also consistent with recent theoretical results (cf. Dziembowski & Pamyatnykh 1993 and Gautschy & Saio 1993) showing that the metal abundance parameter Z = 0.02 is sufficient for driving pulsations in β Cephei stars. Finally, an analysis of the H I Ly$_{\alpha}$ line reveals the hydrogen interstellar column density toward δ Cet equal to log N(H I) = 20.0.

Acknowledgements. This work was supported by the research grant No. 2 P03D 001 08 from the Polish Scientific Research Committee (KBN). Stellar models and linear nonadiabatic pulsation data were obtained from Prof. W. Dziembowski and Dr. A. Pamyatnykh. ESA IUE Observatory at VILSPA provided the IUE tapes. To them all, we express our thanks. We also would like to thank the referees for careful reading of the manuscript and for valuable comments. The editorial office kindly made english corrections.

References

Balona L. A., 1994, MNRAS 268, 119
Bohlin R. C., Savage B. D., Drake J. F., 1978, ApJ 224, 132
Bressan A., Fagotto F., Bertelli G., Chiosi C., 1993, A&AS 100, 647
Buser R., Kurucz R. L., 1992, A&A 264, 557
Claret A., Gimenez A., 1992, A&AS 96, 255
Code A. D., Davis J., Bless R. C., Hunbury Brown R., 1976, ApJ 203, 417
Cugier H., 1993, Acta Astron. 43 27
Cugier H., Dziembowski W., Pamyatnykh A. A., 1994, A&A 291, 143
Davis J., Shobbrook, R.F., 1977, MNRAS 178, 651
Dziembowski W., 1994, in Pulsation, Rotation and Mass Loss in Early-Type Stars, IAU Symp. 162, eds. L. Balona, H. Henrichs and J. M. Le Contel (Dordrecht, Kluwer), p. 55
Dziembowski W., 1995, in Astrophysical Applications of Powerful New Databases, ASP Conference Series, Vol. 78, eds. S. J. Adelman and W. L. Wiese, p 275
Dziembowski W., Pamyatnykh A.A., 1991, A&A 248, L11
Dziembowski W., Pamyatnykh A.A., 1993, MNRAS 262, 204
Gautschy A., Saio H., 1993, MNRAS 262, 213
Gies D.R., Lambert D.L., 1992, ApJ 387, 673
Jenkins E.B., 1970, Ultraviolet Stellar Spectra and Related Ground-Based Observations, IAU Symp. No. 36, p. 281
Jerzykiewicz M., Sterken C., Kubiak, M., 1988, A&AS 72, 449
Kolb M., Baade D., 1994, in Pulsation, Rotation and Mass Loss in Early-Type Stars, IAU Symp. 162, eds. L. Balona, H. Henrichs and J.M. Le Contel (Dordrecht, Kluwer), p. 55
Kurucz R.L., 1979a, ApJS 40, 1
Kurucz R.L., 1979b, ApJS 40, 243
Kurucz R.L., 1991, in Precision Photometry: Astrophysics of the Galaxy, eds. A.G. Davis Philip, A.R. Upgren, K.A. Janes (L.Davis Press)
Lester J.B., Gray R.O., Kurucz R.L., 1986, ApJ Suppl. 61, 509
Lindemann E., Hauck B., 1973, A&AS 11, 119
Napiwotzki R., Schonberner D., Wenske V., 1993, A&A 268, 653
Rogers F.J., Iglesias C.A., 1992, ApJS 79,507
Sahal-Brechot S., Segre E.R.A., 1971, A&A 13, 161
Savage B.D., Mathis J.S., 1979, Ann. Rev. Astron. Astrphys. 17, 73
Schaller G., Schaerer D., Meynet, G., Maeder, A., 1992, A&AS 96, 269
Schild R., Peterson D.M., Oke J.B., 1971, ApJ 166, 95
Seaton M.J., Yan Y., Mihalas D., Pradhan A.K., 1994, MNRAS 266, 805
Shaw J.S., 1975, A&A 41, 367
Shobbrook R.F., 1976, MNRAS 176, 673
Shobbrook R.F., 1878, MNRAS 214, 33
Smalley B., Dworetsky M.M., 1995, A&A 293, 446
Stehle C., 1994, A&A Suppl. 104, 509

This article was processed by the author using Springer-Verlag LaTeX A&A style file *L-AA* version 3.